FCP Report No. 7

INTERIM REPORT ON FATIGUE BEHAVIOR OF HIGH HARDNESS NODULAR CAST IRON

by

R. A. Testin
Department of Theoretical and Applied Mechanics

ABSTRACT

Monotonic and fatigue test results on three nodular irons with different mean nodule sizes are reported. Scanning electron microscope studies of the fracture surfaces indicate that the controlling fatigue cracks initiate from the most severe flaw such as microshrinkage cavities, slag inclusions or porosity. The effect of precycling on fatigue life is explored. Predictive techniques sometimes used for estimating the fatigue resistance of wrought metals are shown to be unsatisfactory for this nodular iron.

A Report of the
FRACTURE CONTROL PROGRAM

College of Engineering, University of Illinois
Urbana, Illinois 61801
March, 1973

INTRODUCTION

The mechanical properties of nodular cast iron were reviewed with special reference to fatigue in FCP-2 (1). Since cracks were reported to initiate at the perimeter of nodule sites, it was decided to approach this cast iron as a flawed or internally notched steel. More specifically, the graphite nodules were to be considered as crack initiating, spherical flaws in a steel matrix.

For steels, one empirical relationship between the fatigue strength reduction factor, K_f, and the effective inclusion radius is given as (2):

$$K_f = 1 + \frac{K_t - 1}{1 + \frac{a}{r}} \qquad (1)$$

where K_t = theoretical elastic stress concentration factor

r = inclusion radius, inches

a = structure related material constant approximated* as

$$a \text{ (inches)} = 0.001\,[300/S_u]^{1.8} \qquad (2)$$

S_u = engineering ultimate strength, ksi

If the ultimate strength in ksi is approximated by one-half the Brinell hardness and a K_t value of 2.5 is assumed**, the relationship between K_f, hardness, and inclusion radius is depicted in Fig. 1. This figure indicates that as a steel becomes harder (stronger), it also becomes more notch sensitive, and that a flaw size threshold exists for each hardness above which the flaw becomes highly effective in

---

*Morrow (3) approximated this working relationship from published fatigue data on steel.

**K_t for an axially loaded wide plate with a central hole is three, while for a spherical cavity in a solid matrix it is about two. As a working approximation $K_t \approx 2.5$ is chosen for a spherical nodule near the surface.

reducing fatigue strength. Assuming nodular iron behaves similarly to a notched steel, it was felt that by varying nodule size, different values of K_f would result, and these K_f values could be predicted from the properties of the matrix material.

Deere and Company cast three irons of approximately the same composition, and achieved different nodule sizes by controlling cooling rates and inoculation procedures. The irons were heat treated to the same structure and hardness.* Composition, heat treatment, hardness, and mean nodule size data are reported in Table 1. Micrographs of the structure are given in Fig. 2 for each of the irons tested.

METHOD OF TESTING

Axially loaded smooth specimens with cylindrical test sections, shown in Fig. 3, were tested. All monotonic tension and fatigue tests were performed on a push-pull MTS closed-loop, servo-controlled hydraulic testing system. Strains were measured using either an Instron clip gage over a 0.75 in. gage length or a MTS clip gage over a 0.50 in. gage length. Strain was controlled during all low cycle testing and all precycling; stress was controlled for long life tests. Compression tests were conducted on a Riehle Universal Testing Machine.

TEST RESULTS

Monotonic tension tests were performed on each of the nodular irons. Compression tests were conducted on cylindrical specimens with an ℓ/d ratio of 1.75. Monotonic properties of the three irons are reported in Table 2.

---

*The hardness at which the nodule size effect would be distinguishable according to Fig. 1; a fine pearlite with no "bullseyes" was the desired structure.

Fatigue Test Results

The cyclic stress-strain curves for each of the irons tested are given in Fig. 4. Monotonic stress-strain curves are also shown for comparison. There appears to be little difference between incremental step test results and companion specimen data. Nearly the same cyclic stress-strain response is noted for the medium and large nodule irons, while the curve for the small nodule iron is slightly higher. This difference is actually small, however, and one would not expect large differences in fatigue resistance from these results.* These irons did not cyclically harden or soften to any appreciable extent.

Completely reversed, constant amplitude fatigue testing was conducted on all three nodular irons. The fatigue properties as defined by Raske and Morrow (4) are reported in Table 3. Tests were conducted on specimens that were not precycled as well as specimens that were precycled. Precycling consisted of five cycles at a strain of ± 0.005 followed by incrementally decreasing the strain amplitude to zero in about 40 reversals. Figure 5a illustrates a typical strain-time and load-time record for the precycling sequence and Fig. 5b shows the stress-strain response of the nodular iron during precycling. It was found that for the medium nodule size, precycling improved fatigue lives in all cases (Fig. 6). This is contrary to what one would expect since precycling generally has a detrimental effect on fatigue life for most steels (5). The precycling technique is thought to eliminate possible residual stresses around the "flaws" in the material. Results suggest that a tensile residual stress exists around the internal notches due to the solidification or heat treatment process. All subsequent specimens were precycled.

---

*Note: This slight difference could be due to the slightly higher Si content (2.75%) of the small nodule iron.

Completely reversed, constant amplitude strain-life data for the three nodular irons are presented in Table 4 and plotted in Fig. 7. Nodule size does not appear to significantly affect the fatigue life, which suggests that "flaws" larger than the nodules govern fatigue behavior.

MICROSCOPIC STUDIES

Fracture specimens having well-defined crack growth regions were examined using the scanning electron microscope (SEM). Failure related cracks were found to initiate from flaws such as microshrinkage cavities, slag inclusions, or porosity rather than from the nodules. Photographs of these "starter flaws" are shown in Figs. 8a-e. Figure 9 indicates a potentially hazardous cluster of nodules which would have a more severe stress concentrating effect than an individual nodule. Porosity in etched and polished specimens is shown in Fig. 10. Fatigue striations, which are often evident in cast steel or wrought steel fatigue failures and are not present in gray iron fatigue failures (6), were not distinguishable in the crack growth region. Evidence that crack propagation is a linking phenomenon for nodular iron is given in Fig. 11. This area was away from the most severe flaw (which had a well defined initiation site, Fig. 8c), and indicates that crack fronts joined across parallel planes.

PREDICTIVE TECHNIQUES

While fatigue life predictions based on monotonic properties* are reasonably accurate (and convenient) for wrought metals, it is unlikely that these techniques have direct applicability to heavily flawed materials such as cast irons. Figure 12 compares the actual strain-life data for the irons tested and predictions based on

*Two of these methods are described in Appendix 1.

the techniques presented in the Appendix. Predictions based on monotonic properties may be more reasonable for lower hardness cast irons, but these methods have been shown to be unsatisfactory for gray irons (6, 8). The results of this investigation indicate that it is necessary to characterize the controlling flaws in order to make accurate fatigue life predictions; once the most critical flaw is classified (K_f), it should be possible to predict fatigue behavior from the properties of the matrix material.

CONCLUSIONS

Monotonic and fatigue tests have been conducted on three nodular irons with the same structure and different mean nodule sizes. These properties are reported along with strain-life data for each of the irons. Fracture surfaces of fatigue specimens with well defined crack growth regions have been examined using the scanning electron microscope in order to determine the starter flaw.

(1) Although results in the literature indicate initiation of cracks at nodule sites, failure related cracks initiate from the most severe flaw such as microshrinkage cavities, slag inclusions, or porosity.

(2) There is no difference in the fatigue resistance due to nodule size for the reasons given in conclusion (1).

(3) Precycling appears to increase fatigue life; this is possibly due to the elimination of a tensile residual stress, which could arise around the flaws in the iron during heat treatment.

(4) Evidence that crack propagation is a linking phenomenon is presented.

(5) Predictive techniques which give reasonable fatigue life predictions for wrought metals are, in general, not applicable to internally notched materials such as cast iron. Fatigue life predictions for flawed materials should not be based on bulk properties when flaw and matrix characteristics are known.

ACKNOWLEDGMENT

The author is indebted to Mr. Norman Lillybeck and Deere and Company for casting the nodular irons tested in this program. Technical assistance from Mr. S. J. Stadnick on the scanning electron microscope and Mr. J. F. Martin on the MTS test system is gratefully acknowledged. Thanks are also due Professor JoDean Morrow and Mr. M. R. Mitchell for their many helpful suggestions throughout this investigation.

The author also expresses his thanks to Mrs. R. A. Mathine, who typed the manuscript.

REFERENCES

1. Testin, R. A., "A Review of the Mechanical Properties of Nodular Cast Iron with Special Reference to Fatigue," FCP No. 2, College of Engineering, University of Illinois, March, 1972.

2. Peterson, R. E., Metal Fatigue, Chapt. 13, "Notch-Sensitivity," Sines and Waisman, ed., McGraw-Hill Book Co., 1959, pp. 293-306.

3. Morrow, JoDean, "Fatigue Properties of Metals," Section 3.2 of SAE Fatigue Design Handbook, Vol. 4, 1968.

4. Raske, D. T. and Morrow, JoDean, "Mechanics of Materials in Low Cycle Fatigue Testing," Manual on Low Cycle Fatigue Testing, ASTM STP 465, American Society for Testing and Materials, 1969, pp. 1-25.

5. Dowling, N. E., "Fatigue Life and Inelastic Strain Response Under Complex Histories for an Alloy Steel," T. & A. M. Report No. 354, Department of Theoretical and Applied Mechanics, University of Illinois, Urbana, Illinois.

6. Mitchell, M. R., "Cyclic Deformation and Fracture Behavior of Gray Cast Iron," M. S. Thesis, College of Engineering, Wayne State University, Detroit, Michigan, 1969.

7. Tetelman, A. S. and McEvily, A. J., Jr., Fracture of Structural Materials, John Wiley and Sons, New York, 1967, pp. 376-379.

8. Richard, T. G. and Sandor, B. I., "The Cyclic Stress-Strain Response of High Strength Cast Iron," Mechanical Behavior of Materials, Vol. II, Society of Materials Science, Japan, 1972, pp. 344-351.

APPENDIX

PREDICTIVE TECHNIQUES FOR ESTIMATING FATIGUE RESISTANCE FROM MONOTONIC PROPERTIES

Two techniques for predicting resistance to cyclic deformation are presented: the universal slopes method and a general method based on both the cyclic stress-strain curve and monotonic fracture properties. Both techniques are currently used for wrought steels and other ductile metals.

Manson's Universal Slopes Method (7)

The cyclic plastic strain range, $\Delta \epsilon_p$, is related to the number of cycles to failure, N_f, by the relationship:

$$\Delta \epsilon_p = \left(\frac{N_f}{\epsilon_f}\right)^{-0.6} \tag{A-1}$$

where ϵ_f is the true fracture ductility.

The elastic strain range $\Delta \epsilon_e$ is related to cycles to failure by

$$\Delta \epsilon_e = 3.5 \frac{S_u}{E} (N_f)^{-0.12} \tag{A-2}$$

where S_u is the ultimate tensile strength and E is the elastic modulus.

Adding the above two equations gives the expression for total strain range as a function of S_u, E, ϵ_f, and N_f

$$\Delta \epsilon = 3.5 \frac{S_u}{E} (N_f)^{-0.12} + \epsilon_f^{0.6} (N_f)^{-0.6} \tag{A-3}$$

In terms of reversals*, which is sometimes used due to its applicability to cumulative damage analysis, this equation becomes

---

*For completely reversed, constant amplitude testing, the number of reversals to failure is equal to twice the number of cycles to failure; hence, $2N_f$ = reversals to failure in a constant amplitude test.

$$\frac{\Delta \epsilon}{2} = 1.9 \frac{S_u}{E} (2N_f)^{-0.12} + 0.75 \epsilon_f^{0.6} (2N_f)^{-0.6} \qquad \text{(A-4)}$$

where $\frac{\Delta \epsilon}{2}$ is the total strain amplitude and $2N_f$ is the number of reversals to failure.

The prediction for nodular iron based on this method is shown in Fig. 12.

Method Based on Cyclic Stress-Strain and Monotonic Properties (3)

For this method it is necessary to know the elastic modulus, E, the cyclic strain hardening exponent, n', the true fracture strength, σ_f, and the true fracture ductility, ϵ_f, of the metal. The cyclic plastic strain amplitude, $\frac{\Delta \epsilon_p}{2}$, can be related to reversals to failure, $2N_f$, by

$$\frac{\Delta \epsilon_p}{2} = \epsilon_f (2N_f)^c \qquad \text{(A-5)}$$

where c is the fatigue ductility exponent.

The cyclic elastic strain amplitude can be related to reversals to failure by

$$\frac{\Delta \epsilon_e}{2} = \frac{\sigma_f}{E} (2N_f)^b \qquad \text{(A-6)}$$

where b is the fatigue strength exponent.

Combining the above two equations, we have the expression for total strain amplitude as a function of reversals to failure:

$$\frac{\Delta \epsilon}{2} = \frac{\sigma_f}{E} (2N_f)^b + \epsilon_f (2N_f)^c \qquad \text{(A-7)}$$

For most steels the fatigue strength at 10^6 reversals is about $\frac{S_u}{2}$. It is now possible to calculate b.

$$b = -\frac{1}{6} \log \left(\frac{2\sigma_f}{S_u}\right) \qquad \text{(A-8)}$$

From this we can find c, since

$$n' \simeq \frac{b}{c} \tag{A-9}$$

The prediction can now be made knowing σ_f, S_u, ϵ_f, b, and c. The results of this method for nodular iron are shown in Fig. 12.

TABLE 1

COMPOSITION, HEAT TREATMENT, HARDNESS, AND MEAN NODULE SIZE DATA

Average Composition

Total Carbon	3.57%
Graphitic Carbon	2.71
Combined Carbon	0.86
Mn	0.60
Si	2.4*
Cu	0.27
P	0.010
S	0.013
Ni	<0.05
Cr	0.07
Mo	<0.05
Sn	0.08
Mg	0.05

*The Si content of the small nodule iron was about 2.75%.

Heat Treatment

Bars were austenitized for 1 hour at 1700° F, then transferred to a salt bath at 1080° F for 15 minutes. They were then air cooled to room temperature. Bulk hardness: 337 BHN; matrix hardness: 352 BHN.

Mean Nodule Size Data

Nodule Size	Radius, in.	Volume Fraction Graphite
Small	0.0004	~10%
Medium	0.0007	~10%
Large	0.0013	~10%

TABLE 2

MONOTONIC PROPERTIES

Property	Nodule Size of Cast Iron			
	Small	Medium	Large	Average
Elastic Modulus, E, ksi	25,000	25,000	25,000	25,000
Ultimate Strength				
Tension, S_u, ksi	134	135	125	131
Compression, ksi	344	344	344	344
Yield Strength (0.2%)				
Tension, S_{ys}, ksi	112	101	96	103
Compression, ksi	112	103	98	104
True Fracture Ductility				
Tension, ϵ_f	0.018	0.025	0.020	0.021
Compression	0.09	0.09	0.09	0.09
True Fracture Strength				
Tension, σ_f, ksi	137	139	128	135
Compression, ksi	205	205	205	205 (shear)
Strain Hardening Exponent, n	0.10	0.16	0.16	0.14
Strength Coefficient, K, ksi	210	260	245	240

TABLE 3

FATIGUE PROPERTIES

Property	Nodule Size of Cast Iron			
	Small	Medium	Large	Average
Cyclic Strain Hardening Exponent, n'	0.16	0.20	0.20	0.19
Cyclic Strength Coefficient, K', ksi	280	340	360	325
Fatigue Strength Exponent, b	-0.10	-0.11	-0.11	-0.11
Fatigue Ductility Exponent, c	-0.53	-0.52	-0.53	-0.53
Fatigue Strength Coefficient, σ_f', ksi	180	180	180	180
Fatigue Ductility Coefficient, ϵ_f'	0.045	0.060	0.050	0.052
Transition Fatigue Life, $2N_t$	100	250	120	160

TABLE 4

FATIGUE TEST RESULTS

Specimen*	Total Strain Amplitude $\Delta \epsilon/2$	Reversals to Failure $2N_f$	Remarks
12MR	0.010	12	Not precycled
13SR	0.010	14	Precycled
4M	0.010	20	Precycled
2L7	0.010	30	Precycled
12M	0.010	54	Precycled
1M	0.010	64	Precycled
15M	0.010	80	Precycled
2SR	0.006	284	Precycled
2L15	0.006	318	Precycled
3MR	0.006	388	Not precycled
16S	0.006	500	Precycled
8MR	0.006	824	Precycled
17M	0.006	1,090	Precycled
16M	0.006	1,138	Precycled
16MR	0.004	3,200	Precycled
5MR	0.003	5,000	Precycled
17MR	0.003	6,000	Precycled
3L9	0.003	11,800	Precycled
18S	0.003	15,340	Precycled
14MR	0.003	23,000	Precycled
3L25	0.0025	36,000	Did not fail at ±35 ksi; stress control at ±60 ksi
3L24	0.0021	74,000	Overstrained in tension; stress control at ±50 ksi
1L20	0.0021	153,000	

*In the specimen number, the letter designates small, medium, or large nodule size, R designates riser end of the casting; large nodule irons are from three different slugs (hence, two identifying numbers each).

TABLE 4 (Cont'd.)

FATIGUE TEST RESULTS

Specimen*	Total Strain Amplitude $\Delta\epsilon/2$	Reversals to Failure $2N_f$	Remarks
15MR	0.0020	27,200	Not precycled
8M	0.0020	72,500	Not precycled
13M	0.0020	73,000	Precycled
9MR	0.0020	117,000	Precycled
2L17	0.0020	130,000	Precycled
3L14	0.0020	131,000	Precycled; overstrained in tension; stress control at ±48 ksi
11MR	0.0020	150,000	Precycled
3S	0.0020	235,000	Precycled
3L11	0.0016	0.67×10^6	Precycled; overstrained in compression; stress control at ±35 ksi
2L18	0.0016	0.80×10^6	Not precycled; stress control at ±35 ksi
9S	0.0016	1.53×10^6	Precycled; stress control at ±35 ksi
6M	0.0016	1.81×10^6	Precycled; stress control at ±35 ksi
3L2	0.0015	0.64×10^6	Precycled
1L18	0.0015	0.68×10^6	Precycled
20S	0.0015	5.70×10^6	Precycled
3L25	0.0013	10.5×10^6	Precycled; did not fail; stress control at ±32 ksi; later run at ±60 ksi
10SR	0.0010	10.5×10^6	Precycled; did not fail; stress control at ±25 ksi

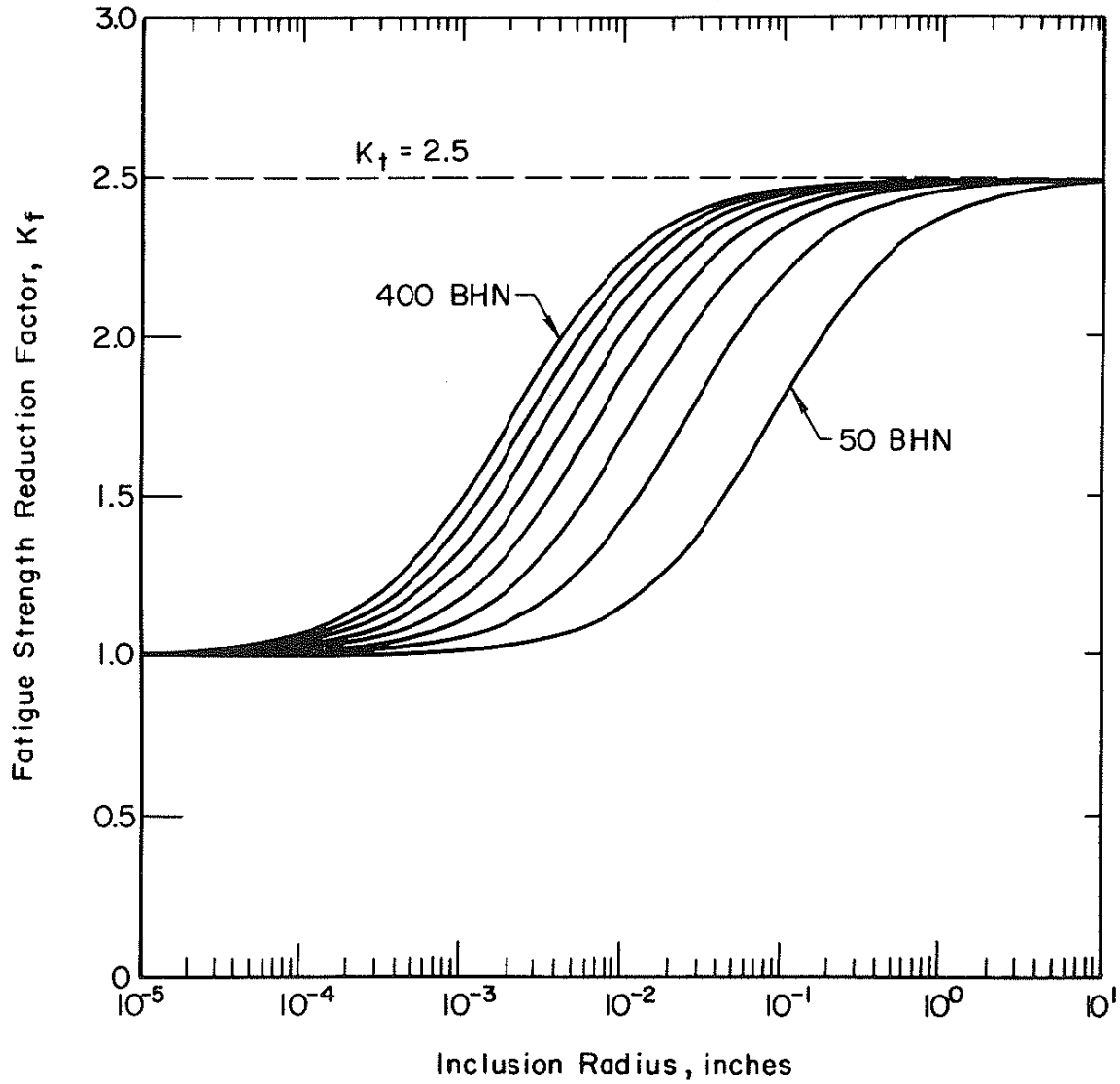

FIG. 1 FATIGUE STRENGTH REDUCTION FACTOR VS. INCLUSION RADIUS FOR STEEL (SEE EQ. 1)

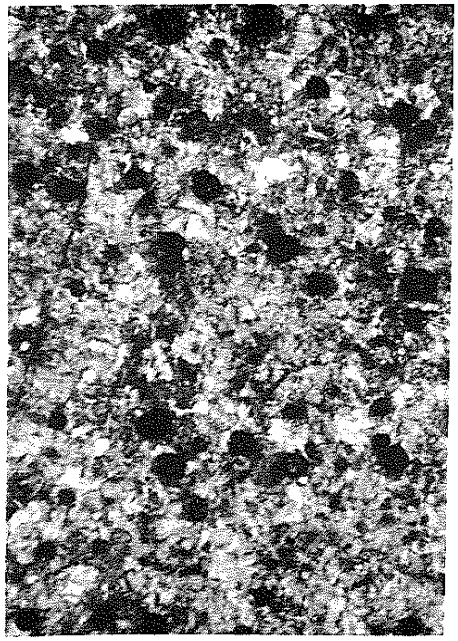

Small

Medium

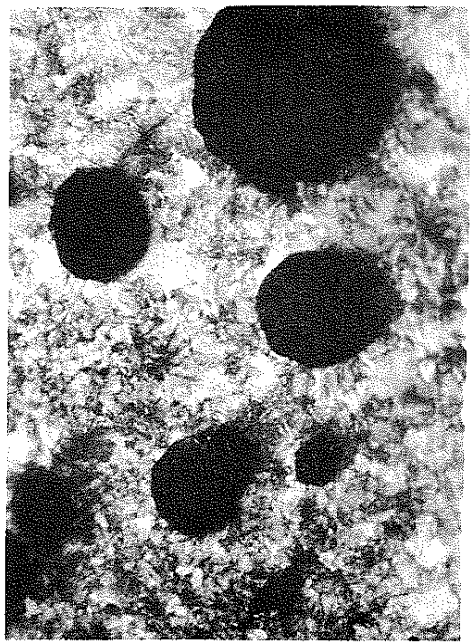

Large

FIG. 2 MICROSTRUCTURES OF THE THREE NODULAR IRONS TESTED

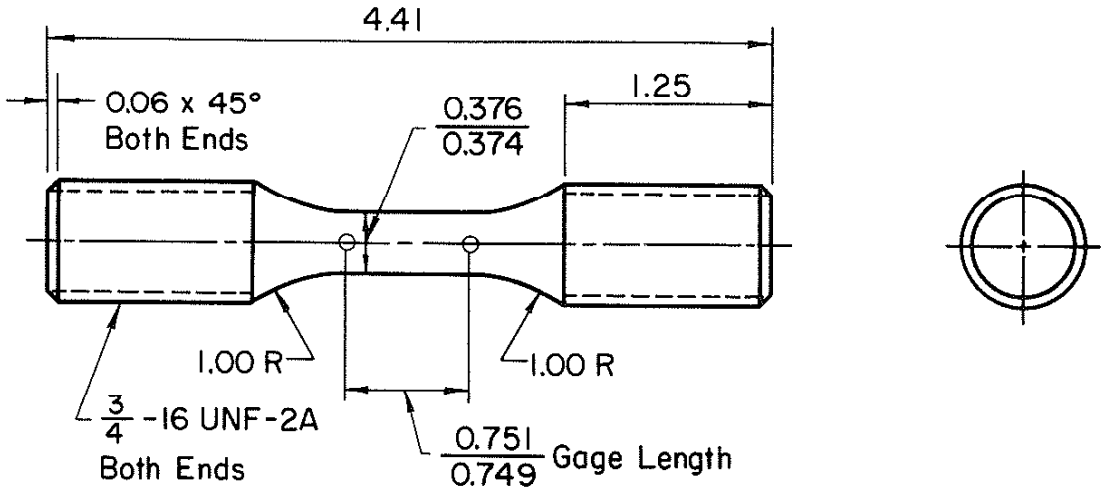

Machined Dim. ± 0.01
Angular Dim. ± 1°

All Dimensions in Inches

FIG. 3 SPECIMEN DESIGN USED FOR MONOTONIC AND CYCLIC TESTS

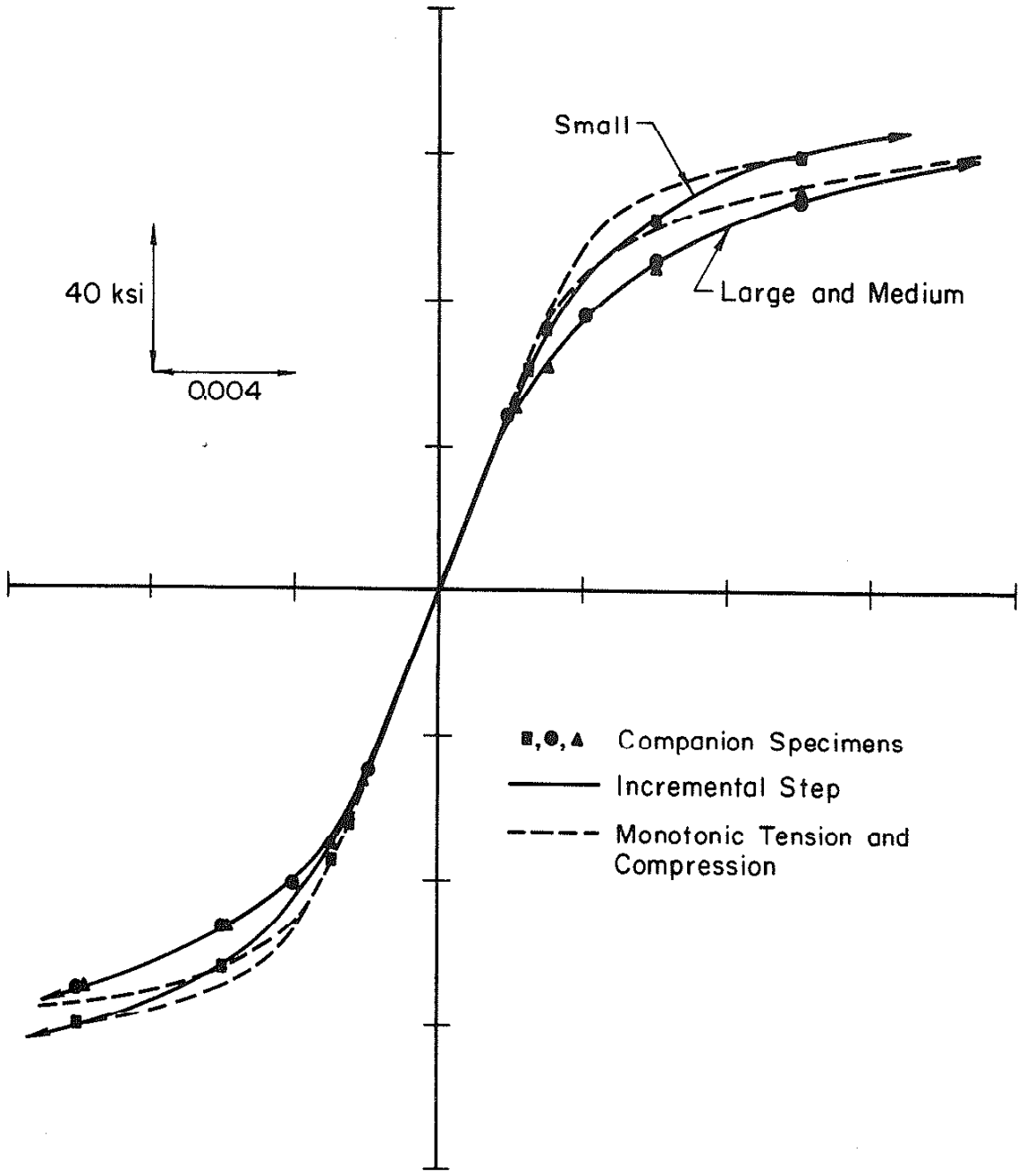

FIG. 4 MONOTONIC AND CYCLIC STRESS–STRAIN CURVES FOR THE THREE NODULAR IRONS

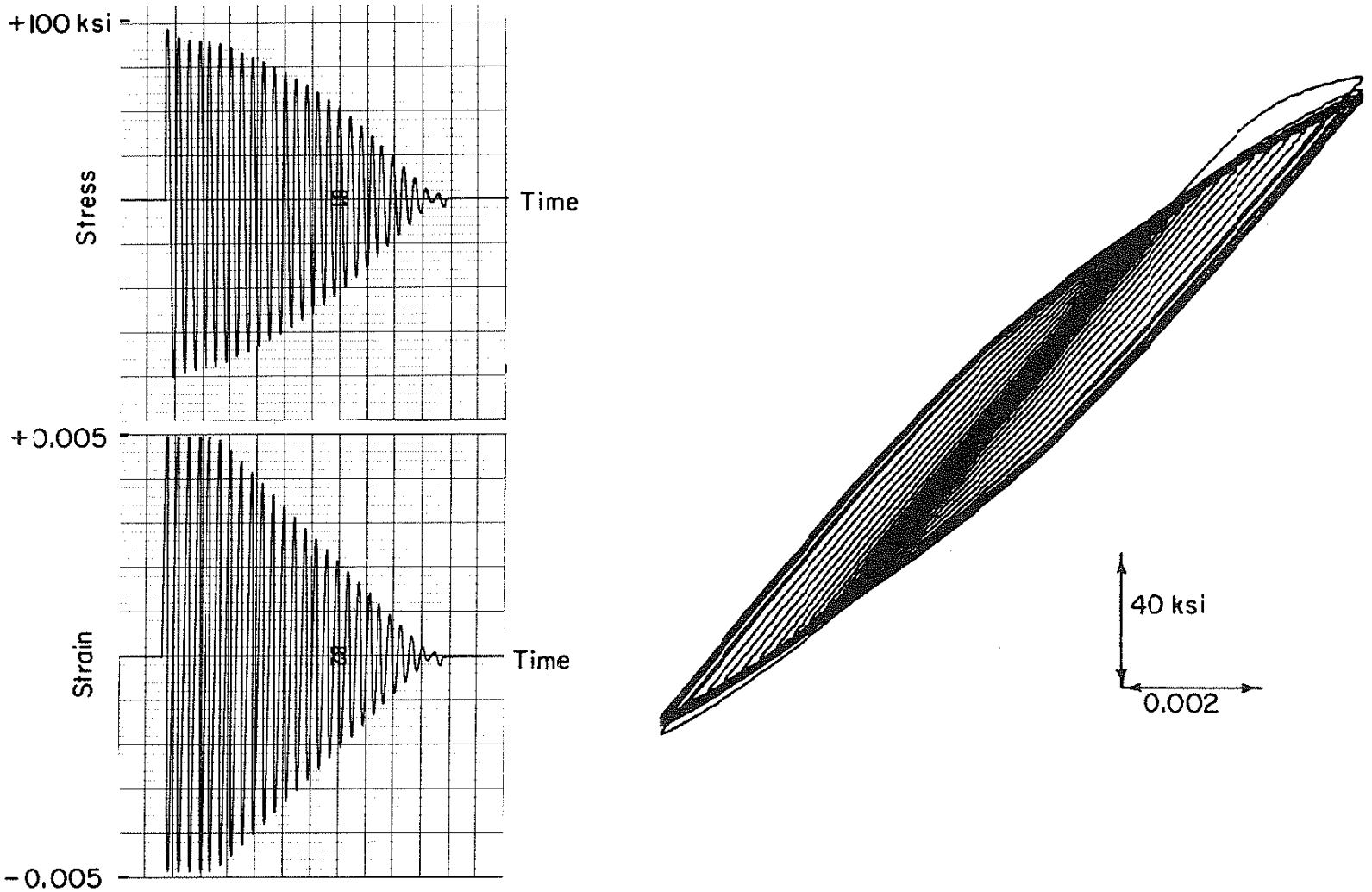

FIG. 5 TYPICAL STRESS AND STRAIN-TIME RECORD AND STRESS-STRAIN RESPONSE FOR PRECYCLING SEQUENCE

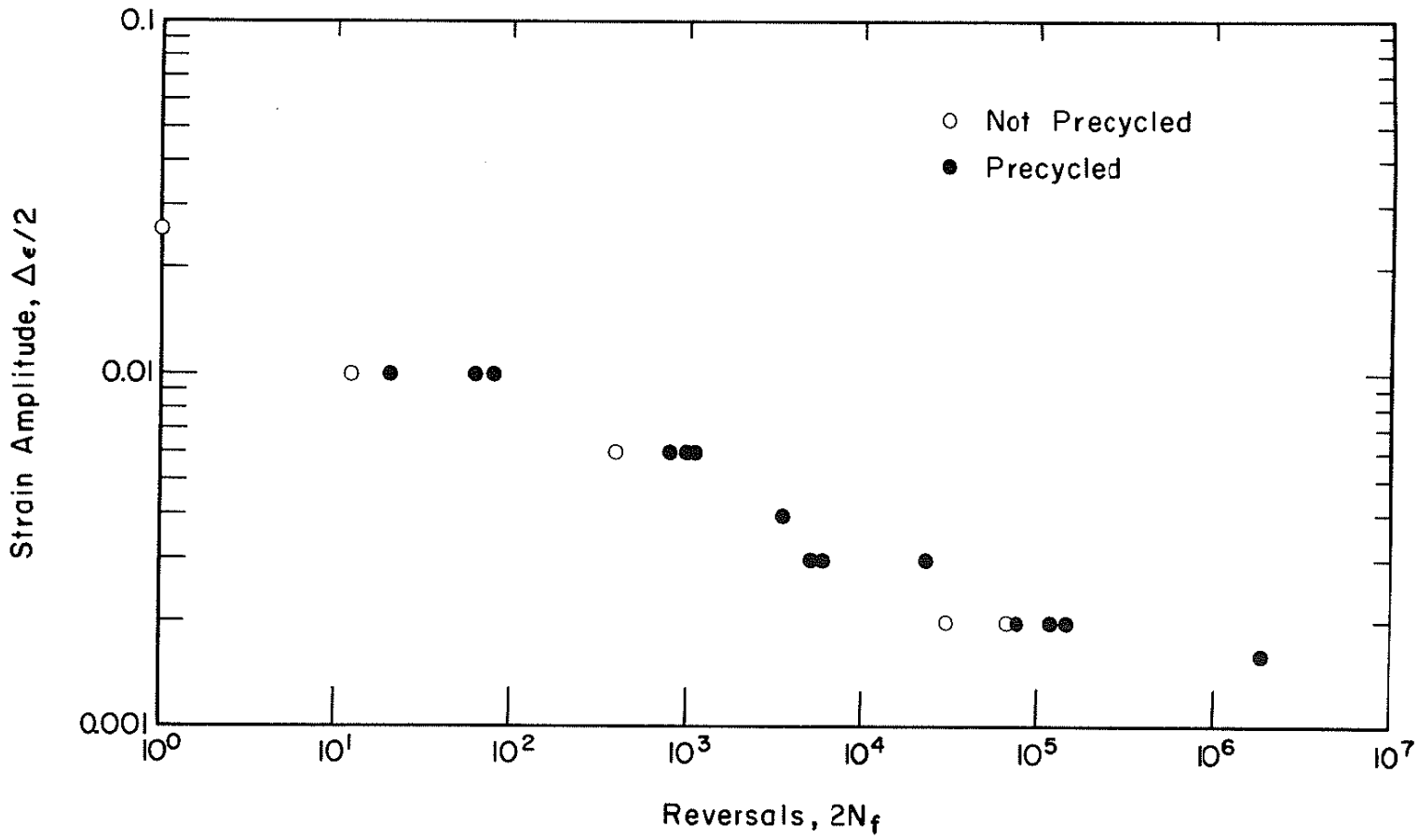

FIG. 6 EFFECT OF PRECYCLING ON FATIGUE LIFE OF MEDIUM NODULE SIZE CAST IRON

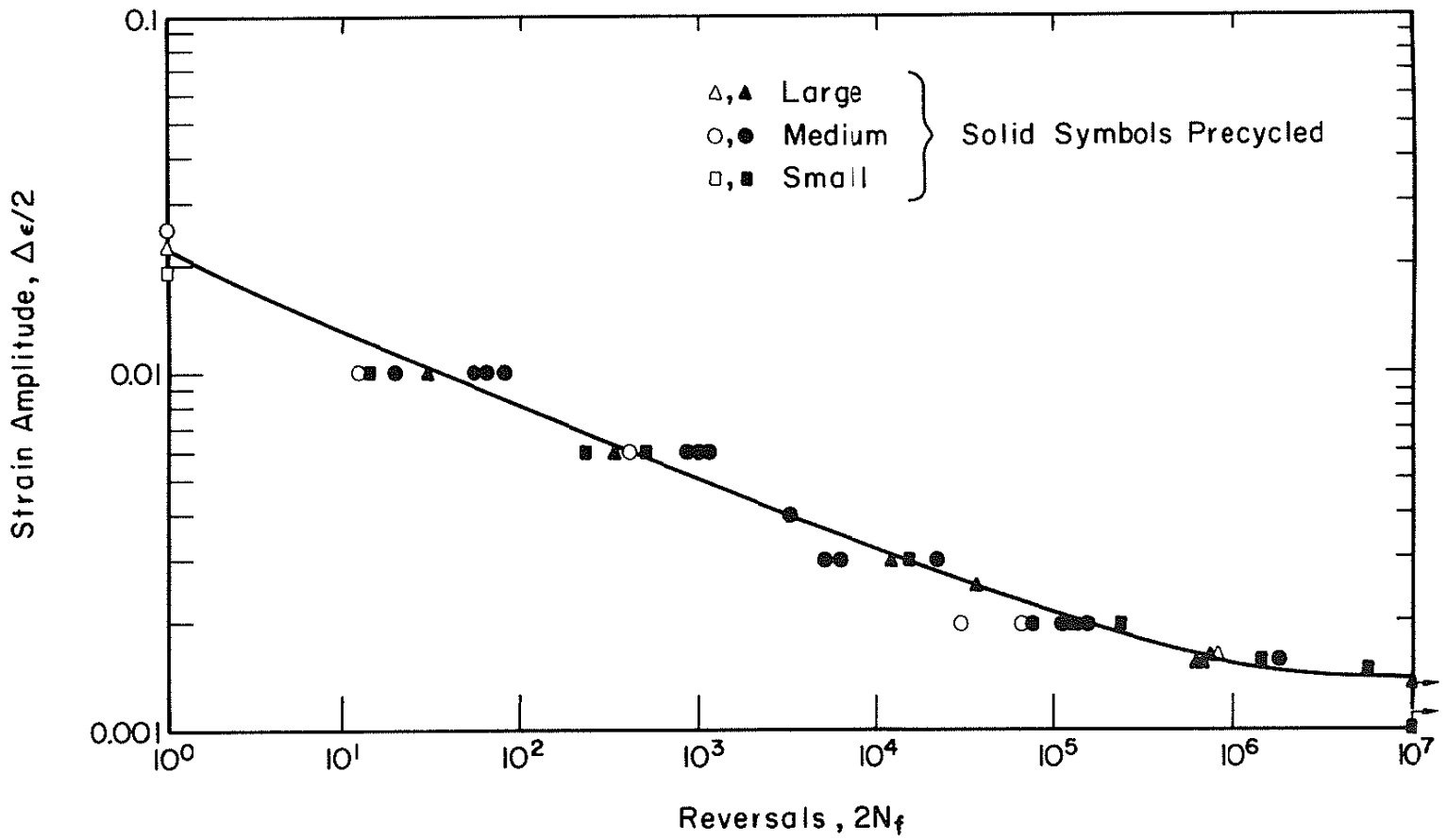

FIG. 7 STRAIN-LIFE DATA FOR SMALL, MEDIUM, AND LARGE NODULE IRONS

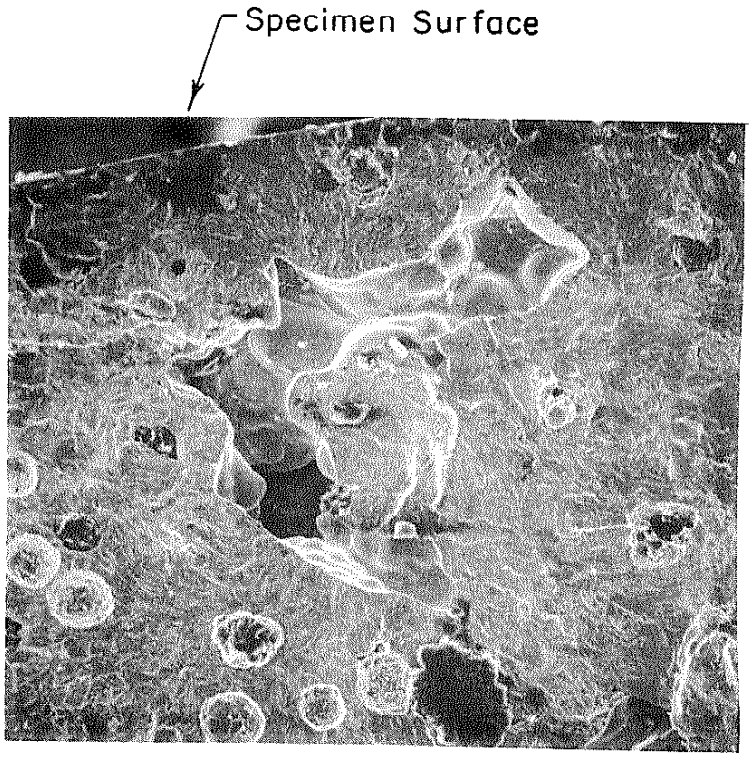

e) Specimen 3L2

FIG. 8 INITIATION POINT OF FATIGUE CRACK

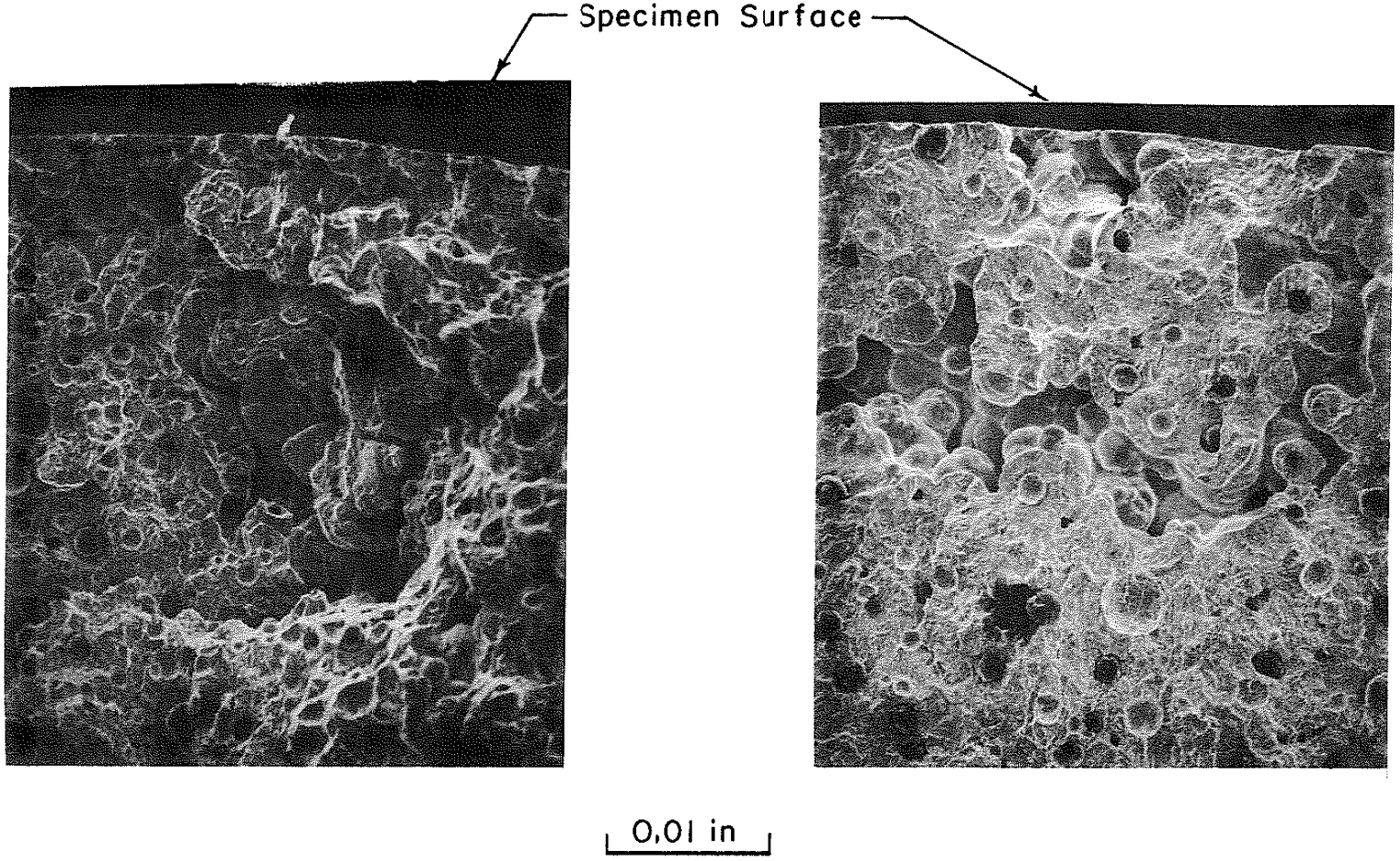

a) Specimen 2S

b) Specimen 9 MR

FIG. 8 INITIATION POINTS OF FATIGUE CRACKS

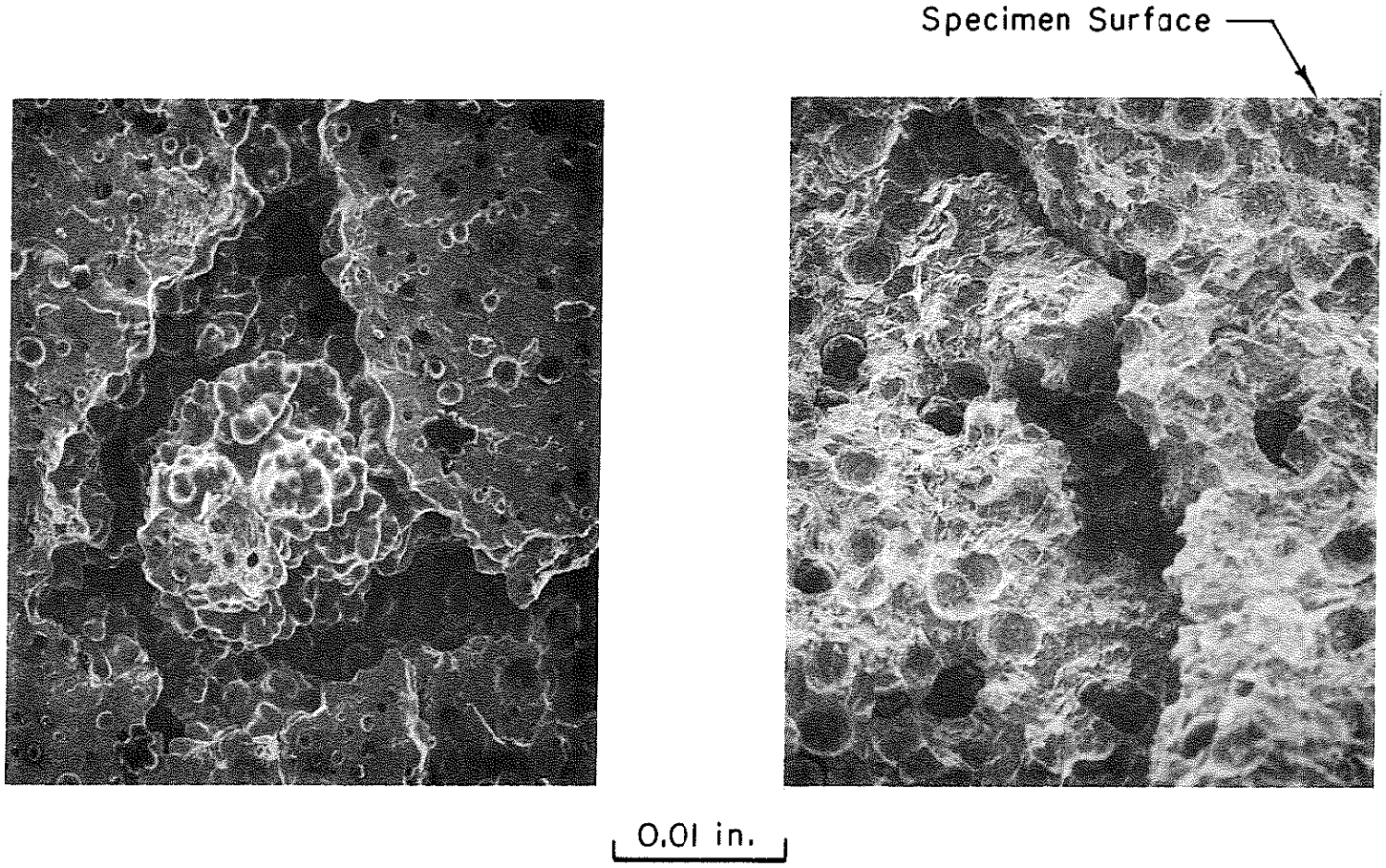

c) Specimen 20S

d) Specimen 2L15

FIG. 8 INITIATION POINTS OF FATIGUE CRACKS

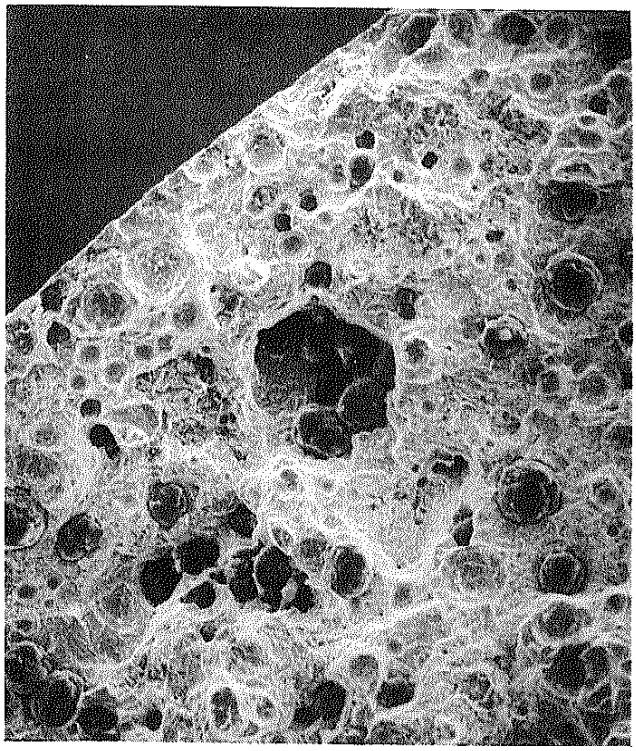

Specimen 9MR

FIG. 9 CLUSTER OF GRAPHITE NODULES

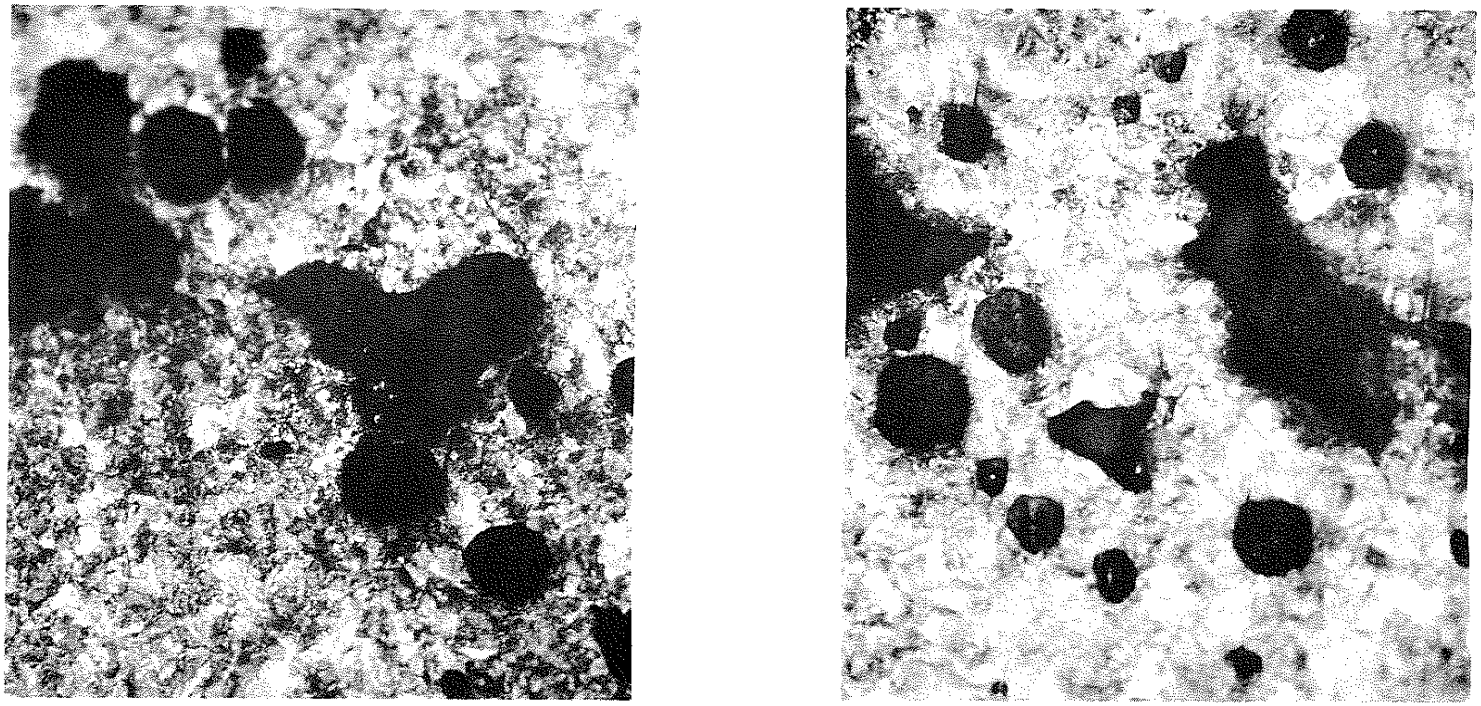

0.005 in.

Specimen 2L17

Specimen 8MR

FIG. 10 POROSITY IN POLISHED AND ETCHED SPECIMENS

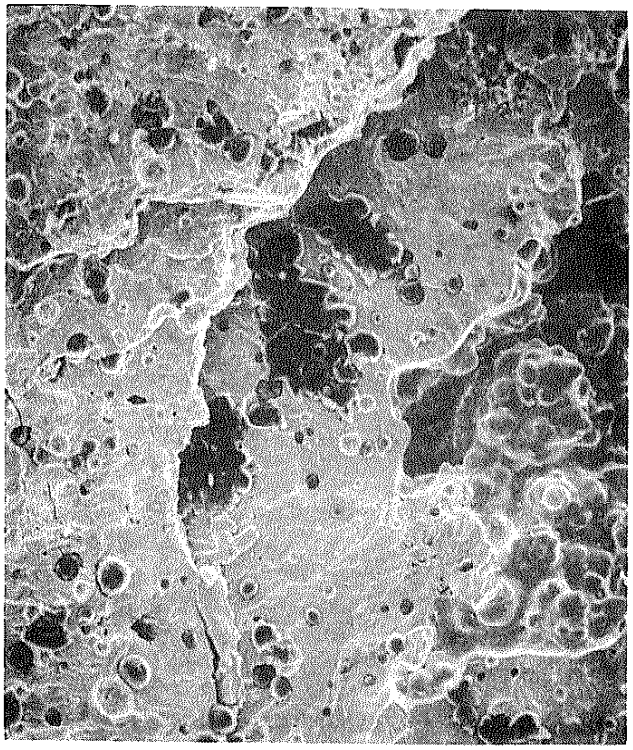

0.01 in.

Specimen 20S

FIG. 11 FRACTURE SURFACE OF SPECIMEN HAVING A DISTINCT "STARTER FLAW" AWAY FROM THIS AREA

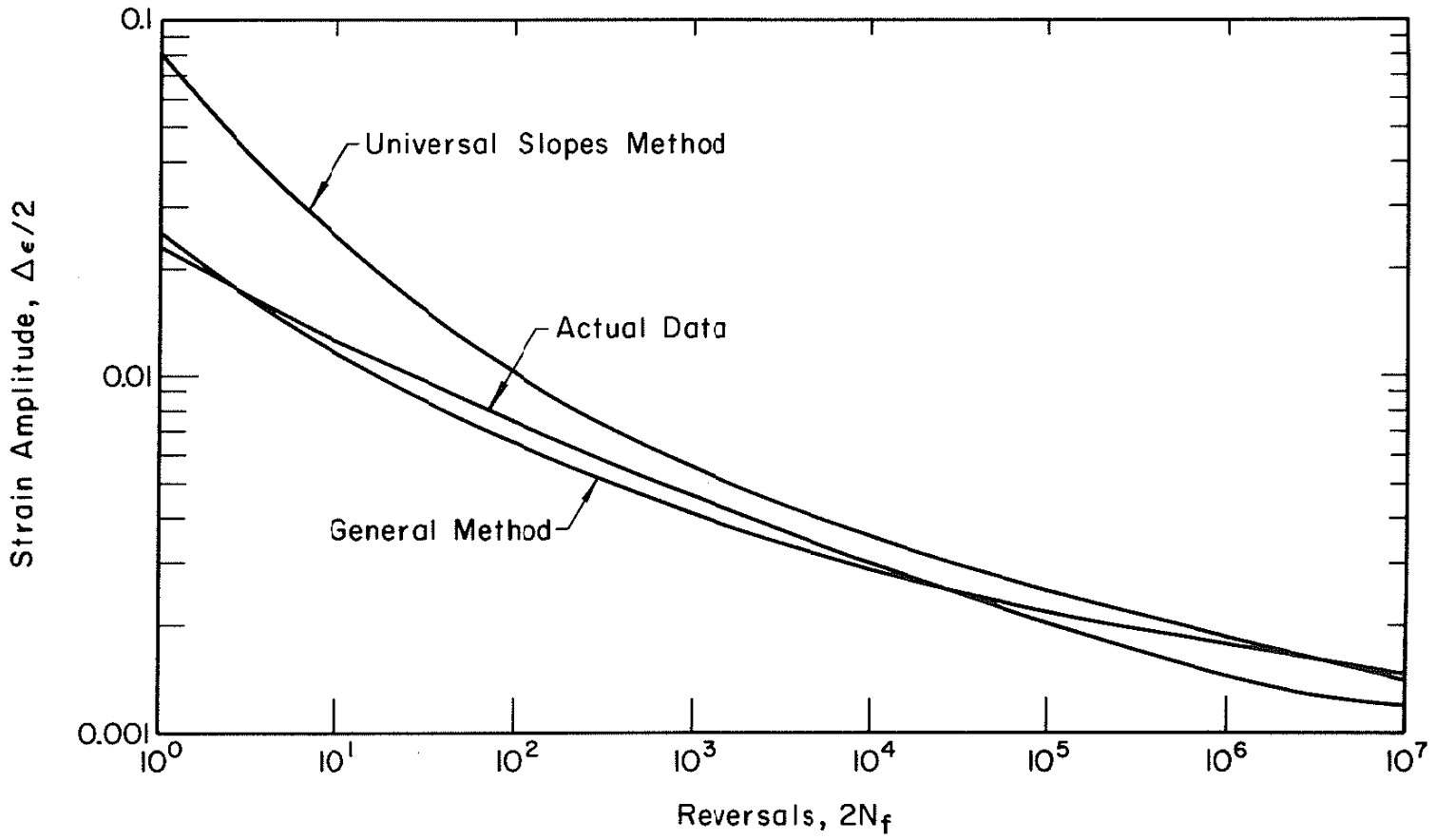

FIG. 12 COMPARISON OF ACTUAL DATA WITH TWO PREDICTIONS BASED ON MONOTONIC PROPERTIES (SEE APPENDIX)